

# Novel Polyepoxysuccinic Acid-Grafted Polyacrylamide as a Green Corrosion Inhibitor for Carbon Steel in Acidic Solution

Rem Jalab, Ahmed Ben Ali, Mazen Khaled,\* Maha Abouseada, Safa AlKhalil, Amna Al-Suwaidi, Sali Hamze, and Ibbelwaleed A. Hussein\*



Cite This: *ACS Omega* 2023, 8, 16673–16686



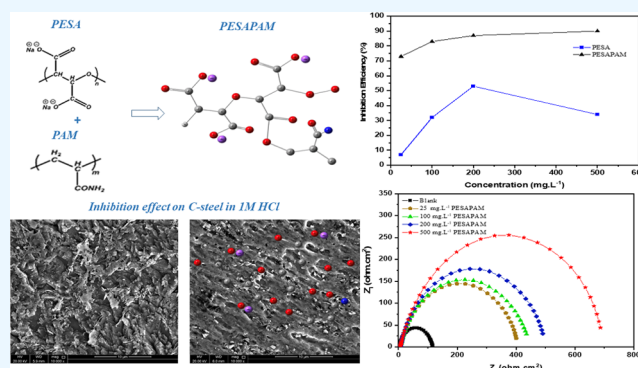
Read Online

ACCESS |

Metrics & More

Article Recommendations

**ABSTRACT:** Utilizing green corrosion inhibitors has been classified among the most efficient and economical mitigation practices against metallic degradation and failure. This study aims to integrate the features of green and complementary properties of polyepoxysuccinic acid (PESA) and polyacrylamide (PAM) for steel corrosion inhibition. A novel PESA-grafted-PAM (PESAPAM) has been first-ever synthesized in this research study and deployed as a corrosion inhibitor for C-steel in 1.0 M HCl solution. Eco-toxicity prediction confirmed the environmentally friendly properties acquired by the synthesized inhibitor. Electrochemical, kinetics, and surface microscopic studies were carried out to gain a holistic view of C-steel corrosion behavior with the PESAPAM. Furthermore, the performance of PESAPAM was compared with that of the pure PESA under the same testing conditions. Results revealed predominant inhibitive properties of PESAPAM with an inhibition efficiency (IE) reaching 90% at 500 mg·L<sup>-1</sup> at 25 °C. Grafting PAM onto the PESA chain showed an overall performance improvement of 109% from IE% of 43 to 90%. Electrochemical measurements revealed a charge transfer-controlled corrosion mechanism and the formation of a thick double layer on the steel surface. The potentiodynamic study classified PESAPAM as a mixed-type inhibitor. Furthermore, the investigation of C-steel corrosion kinetics with the presence of PESAPAM predicted an activation energy of 85 kJ·mol<sup>-1</sup>, correlated with a physical adsorption behavior. Finally, performed scanning electron microscopy and energy-dispersive X-ray analyses confirmed the adsorption of PESA and PESAPAM, with superior coverage of PESAPAM onto the steel surface.



## 1. INTRODUCTION

The broad utilization of carbon steel (C-steel) in several industrial applications stimulates the increasing need to investigate its corrosion behavior in different media. C-steel is the most employable material for water transport, construction, and, most notably, the oil and gas transportation pipelines, owing to its durable mechanical properties, abundance, and cost efficiency, especially compared to the costly corrosion-resistant alloys.<sup>1</sup> Despite these preferred features, C-steel is readily susceptible to corrosion when immersed in aggressive acidic environments.<sup>2</sup> Treatment processes of oil-well acidizing, acid pickling, and descaling implement the injection of several mineral acids rather than alkaline solutions, to properly eliminate deposits and enhance recovery.<sup>3,4</sup> Steel pipeline cleaning processes to remove precipitated layers are commonly conducted using a 1.0 M HCl solution.<sup>5</sup> Nevertheless, the oil-well acidification is based on injecting (15–28 wt %) HCl solution for flow enhancement.<sup>6</sup>

Corrosion costs around 3–4% of the world's GDP annually, with a significant contribution of approximately 170 billion USD from the oil and gas sector and 463 million USD from downhole corrosion precisely.<sup>7–10</sup> Recent corrosion mitigation practices showed the potential of saving up to 35% of annual corrosion costs, estimated at 875 billion USD.<sup>11</sup> Mitigation of corrosion has been receiving substantial attention to minimize economic losses and environmental and safety concerns.<sup>12</sup> Deposited corrosion products could adversely contaminate the transported materials (liquid or gas), affecting the quality and machinery performance. Furthermore, the leakage of toxic materials from transportation pipelines is accompanied by many environmental problems.<sup>6</sup> Among the several applied

**Received:** November 28, 2022

**Accepted:** January 25, 2023

**Published:** May 2, 2023



strategies to overcome the corrosion problem, the injection of corrosion inhibitors (CIs) is the most efficient and economical mitigation approach.<sup>13</sup> CIs have become effective in preventing steel corrosion by forming a protective film layer, thereby impeding the direct contact of the metal surface with the surrounding corrosive medium. The adsorption of CIs is generally facilitated by the presence of  $\pi$ -electrons, heteroatoms (N and O), aromatic rings, and polar functional groups in their molecular structure, which act as electron donor sites.<sup>14</sup> Nevertheless, the significant shortcomings of utilizing organic and heterocyclic compounds are their nonenvironmentally friendly nature and synthesis using toxic reactants, solvents, or catalysts. Another disadvantage is the small molecular size, which does not provide sufficient surface coverage.

Literature studies display the versatility of both natural and synthetic polymers in aggressive corrosive environments.<sup>15</sup> Polymeric inhibitors, consisting of several repeating subunits, have expansive properties to distinguish their performance in overcoming corrosion.<sup>16</sup> The hydrophilic and hydrophobic properties of polymers usually determine the stability of adsorbing polymers onto the metal surface. Homopolymers, including polyacrylamide, polyvinylpyrrolidone, polyacrylic acid, and polyvinyl imidazoles, show successful retardation of corrosion, as reported in the literature.<sup>17–21</sup>

Over the years, research approaches have been devoted to exploring environmentally friendly polymeric inhibitors owing to the growing awareness and constrained environmental legislation. Concerns about toxicity and nonenvironmental friendliness attributes of inhibitors can be minimized by employing natural polymers derived from chitosan, cellulose, amino acids, and plant extracts.<sup>16,22</sup> Nonetheless, green chemistry synthesis principles would be preferred for developing green synthetic inhibitors. One-step multicomponent reactions, ultrasound, and microwave irradiation have emerged as the most eco-friendly synthesis protocols for the production of green compounds.<sup>23,24</sup> Ionic liquids,<sup>25</sup> polyethylene glycol,<sup>26</sup> and carbon quantum dots (CQDs)<sup>27</sup> are evaluated as nontoxic inhibitors, demonstrating promising potential.

Among the synthetic green inhibitors, poly(aspartic acid) (PASP) and polyepoxysuccinic acid (PESA) have attracted extensive interest for their environmental acceptance and biodegradability.<sup>28</sup> PESA is a nonphosphorous and nitrogen-free compound that is featured with the chelating and dispersing abilities arising from the existing carboxylic groups in its structure.<sup>29</sup> Commonly, it is classified as an advantageous inhibitor for mineral scales in a wide application range.<sup>30</sup> The outstanding performance of PESA encouraged extending its feasibility investigation in corrosion application. The electrochemical investigation of C-steel corrosion in cooling water revealed a 70% inhibition efficiency for 200 mg·L<sup>-1</sup> PESA.<sup>31</sup> Also, Zhang et al.<sup>32</sup> disclosed a 75% inhibition efficiency of 200 mg·L<sup>-1</sup> PESA for C-steel in soft water. However, another published study demonstrated a 70% inhibition of a novel modified PESA at a considerably lower concentration of 60 mg·L<sup>-1</sup> for low C-steel tested.<sup>33</sup> A recently released research shows the successfulness of thiourea-modified PESA in inhibiting the corrosion of C-steel by 95.6% efficiency.<sup>34</sup> It is reported that pure PESA has an inferior inhibition compared to other organic materials unless large quantities are used, which could be improved by compounding it with other agents.<sup>35</sup> Despite the aforementioned performance evaluation

of PESA, there are no available studies to provide an inclusive perception of the inhibitive behavior in an acidic environment.

Polyacrylamide (PAM), the nontoxic and easily degradable water-soluble polymer,<sup>36</sup> has been frequently used to tackle the corrosion of different steel types in acidic media.<sup>37</sup> The adsorption of PAM onto iron in 1.0 M H<sub>2</sub>SO<sub>4</sub> and 3.0 M HCl was studied.<sup>38,39</sup> Beniken et al.<sup>40</sup> evaluated PAM in 1.0 M HCl solution for the C-steel corrosion inhibition based on weight loss and electrochemical techniques. These experiments reported 85% efficiency at  $3 \times 10^6$  mol·L<sup>-1</sup> PAM concentration. Yet, the anticorrosive characteristics of PAM appear to be not very prominent under all testing conditions. Therefore, graft polymerization was introduced as a practical method for improving the inhibitive performance of PAM. For instance,  $\beta$ -cyclodextrin grafted polyacrylamide achieved 93% efficiency in reducing the X80 steel corrosion at 20 °C.<sup>41</sup> Additionally, nonanyl carboxy methylcellulose-grafted polyacrylamide exhibited a 99.1% anticorrosion protection of AISI-stainless steel in 3.5% NaCl with 1.0 M HCl.<sup>42</sup> PAM grafted onto gums has been documented for corrosion inhibition evaluation in acidic solution.<sup>43,44</sup>

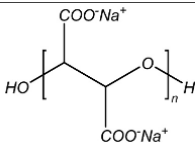
In light of the above, the present study aims to incorporate the environmentally friendly merits of PESA and PAM polymers through a novel PESA-grafted-PAM (PESAPAM) structure for corrosion application. For the first time, the unique environmentally friendly PESAPAM compound is synthesized and investigated for corrosion of C-steel in 1.0 M HCl medium. First, the eco-toxic properties of PESA and PESAPAM are assessed using a specialized web tool. The inhibitive properties of PESAPAM at different concentrations are evaluated by electrochemical impedance spectroscopy (EIS) and potentiodynamic polarization techniques. In addition, a comparative analysis is performed at the same studied concentrations for the PESA inhibitor before grafting. Furthermore, this work also estimates the corrosion kinetics in the presence of PESAPAM at elevated temperatures. Finally, the effect of PESA and PESAPAM on C-steel is also interpreted from the perspectives of microscopic surface characterization and contact angle measurements to correlate surface hydrophobicity with the corrosion inhibition mechanism.

## 2. MATERIALS AND METHODS

**2.1. Steel Samples and Corrosive Solution.** C-steel specimens cut from AISI 1020 alloy sheets were provided by Qatar Steel Co., Ltd., Qatar. The composition of C-steel (wt %) consists of 0.2% carbon with up to 0.7% manganese, 0.65% silicon, and 0.65% copper, and the balance is iron. The polishing of C-steel specimens was carried out using silicon carbide (SiC) abrasive papers and rubbed to a 1500-grit finish. The polished steel samples were then cleaned using deionized water and ethanol. In the end, the samples were dried at a temperature of 110 °C and stored under vacuum in a desiccator. The corrosive medium used in this work is 1.0 M HCl.

**2.2. Chemicals.** Commercial-grade polymeric material PESA of the specifications presented in Table 1 was purchased from Shandong Gite Chemical Co., Ltd., China. Acrylamide (AM, 98%) and ammonium cerium(IV) nitrate (CAN,  $\geq 99\%$ ) were purchased from Glentham Life Science Ltd., United Kingdom, which were used as received without any further purification. Acetone (99.8%) was also supplied by Chem-Lab, Belgium.

Table 1. PESA Polymeric Inhibitor Specifications

	
Molecular Weight	7000–800
Solid Content	40%
Density	1.3 g/cm <sup>3</sup> (20 °C)
pH	11.5

molecular weight	7000–800
solid content	40%
density	1.3 g/cm <sup>3</sup> (20 °C)
pH	11.5

**2.3. Microwave-Assisted Synthesis of PESA-Grafted-Polyacrylamide (PESAPAM).** The commercial PESA solution was precipitated in acetone, and the solid powder was used to prepare grafted materials. The precipitated powder was collected by filtration and placed in an oven for 24 h at 65 °C. Five grams of AM was dissolved in 10 mL of deionized water. After that, 1 g of PESA and 0.2 g of cerium ammonium nitrate (CAN) were prepared in 50 mL of deionized water. This mixture was placed in a microwave reactor under stirring and irradiation of 600 W of power. After 2 min, the microwave irradiation was paused to add AM solution to the reaction mixture, and the irradiation was continued for a total time of 10 min. The container was cooled, and the resultant solution was diluted, filtered, and precipitated in acetone. The grafted material was collected after drying at 65 °C for 24 h followed by crushing and sieving. The proposed structure of the resultant PESAPAM compound is given in Figure 1.

**2.4. Electrochemical Measurements.** The electrochemical measurements were carried out using a GAMRY 3000 potentiostat/galvanostat/ZRA using the three-electrode cell assembly. A graphite rod and Ag/AgCl electrode were used as counter and reference electrodes, respectively. The working electrode was a C-steel sheet with a 1.0 cm<sup>2</sup> cross-sectional area exposed to the corrosive solution. The electrochemical tests were carried out by adding different PESA and PESAPAM concentrations (0, 25, 100, 200, and 500 mg·L<sup>-1</sup>) based on PESA dry solid content calculations. After that, a double-jacketed three-electrode cell was utilized to perform experiments at variable temperatures of 25, 35, 45, and 55 °C. At first, before any electrochemical measurement, the C-steel specimens were left under an open circuit potential (OCP) for

around 30 min until the potential became stable. EIS experiments were conducted under a potentiostatic condition with a frequency ranging from 100,000 to 0.1 Hz and AC amplitude perturbation of 10 mV. Potentiodynamic polarization tests were performed from –250 to +250 mV cathodic to anodic potential against the OCP at a scan rate of 1 mV·s<sup>-1</sup>. Each experiment was repeated three times to ensure data reproducibility.

**2.5. Material Characterization.** The structures of the commercial polymeric inhibitor PESA and the synthesized PESAPAM were analyzed by Fourier transform infrared spectroscopy (FTIR) using a NICOLET iS10 Thermo Scientific FTIR spectrometer. OMNIC software was utilized to display the FTIR spectrum by running 24 scans with 16 cm<sup>-1</sup> resolution over a wavenumber range of 400–4000 cm<sup>-1</sup>.

**2.6. Surface Characterization.** The C-steel samples abraded to 1500-grit finish were immersed in 1.0 M HCl solution with and without 500 mg·L<sup>-1</sup> PESA and PESAPAM for 6 h at 25 °C. Scanning electron microscopy (FE-SEM, FE-SEM-Nova Nano-450) was used to study the surface topography before and after the corrosion experiments.

**2.7. Eco-Toxicity Assessment.** The toxicity properties of the synthesized polymer were predicted using the ADMETlab 2.0 web tool.<sup>45</sup> The properties of absorption, distribution, metabolism, excretion, and toxicity (ADMET) were determined based on a machine-learning model based on 288,967 collected experimental entries.<sup>46</sup> Furthermore, the water solubility was estimated from the SwissADME website<sup>47,48</sup> based on linear regression of 2874 solubility measurements against nine properties.<sup>49</sup>

### 3. RESULTS AND DISCUSSION

#### 3.1. FTIR Characterization of PESA and PESAPAM.

FTIR spectra of both PESA and PESAPAM materials are shown in Figure 2. For the pure PESA, the large peak at around 3288 cm<sup>-1</sup> is due to O–H stretching vibration of the –COOH group. Peaks at 1590 and 1390 cm<sup>-1</sup> are attributed to the symmetric and anti-symmetric stretching vibration of C=O bonds. The bending vibration peaks of O–H appeared at 1314 and 1070 cm<sup>-1</sup> and are assigned to the stretching vibration peaks of the C–O–C group. On the other hand for PESAPAM, the spectrum clearly marks a C=O stretching vibration of amide groups at 1640 cm<sup>-1</sup>, and the characteristic absorption of N–H appeared in the range of 3100–3500 cm<sup>-1</sup>. The formation of a grafted material was confirmed by the presence of characteristic bands of PESA and PAM in the FTIR spectrum of PESAPAM. The O–H band is shifted from 3288 to 3324 cm<sup>-1</sup>; these groups can react with the vinyl

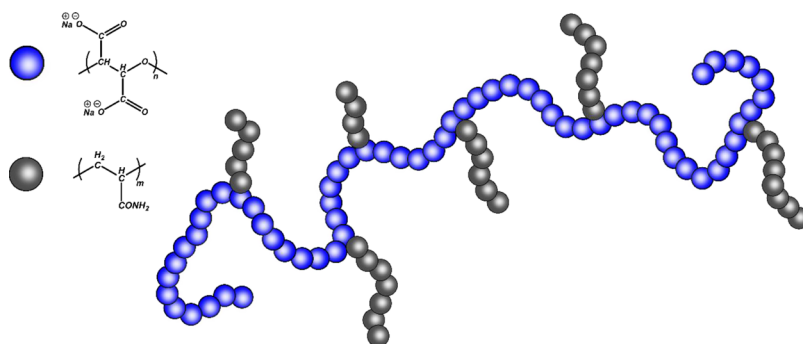
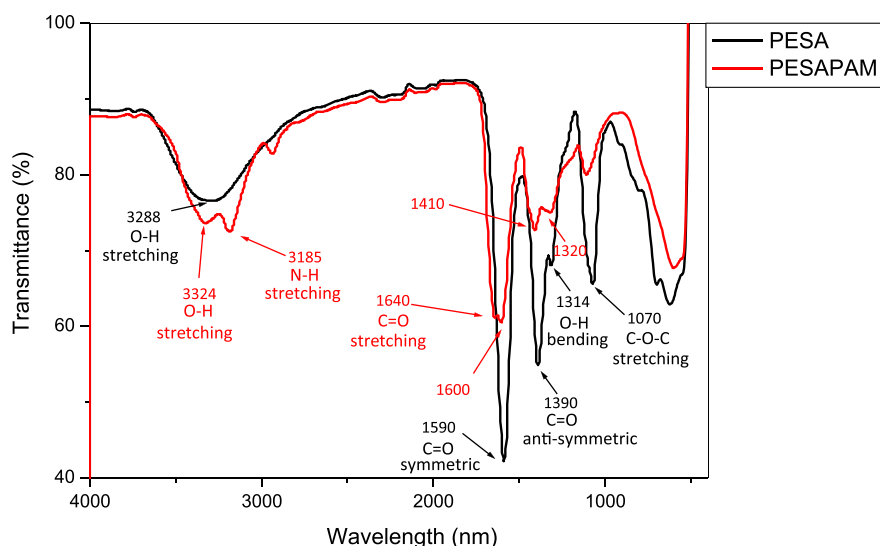


Figure 1. PESAPAM proposed structure.



**Figure 2.** FTIR spectra of PESA and PESAPAM.

groups of AM, thus confirming the formation of PESA-grafted-PAM (PESAPAM). This suggestion is proved by the reduction in intensity and shifting of C=O peaks of COOH from 1590 to 1600  $\text{cm}^{-1}$  and from 1390 to 1410  $\text{cm}^{-1}$ . It is also revealed by the reduction in intensity and the shifting of O–H peaks from 1314 to 1600  $\text{cm}^{-1}$ .

**3.2. Eco-Toxic Evaluation of PESAPAM.** The investigation of eco-toxic parameters is prioritized to confirm the environmental friendliness properties of the synthesized PESAPAM inhibitor. PESAPAM proved to have safe consequences on major ecological parameters studied (Table 2). However, it shows a slightly toxic probability from the aspect of eye corrosion. Indeed, the polymeric inhibitor exhibits a very soluble characteristic in water.

**Table 2. Eco-Toxic Probabilities of the Synthesized PESAPAM Inhibitor**

property	evaluation
carcinogenicity	0.083 (safe)
eye corrosion	0.477 (slightly toxic)
eye irritation	0.096 (safe)
respiratory toxicity	0.01 (safe)
water solubility	−0.14 (very soluble)

**3.3. EIS Measurements.** The impedance spectra of PESA and PESAPAM were obtained from EIS measurements to investigate the effect of inhibitor addition on the corrosion mechanisms.<sup>50</sup> EIS semicircles obtained support understanding the surface-solution interface and electric double layer formed. The double layer formed due to the accumulated species on the metal surface impacts the rate of electron transfer between cathodic and anodic sites.<sup>51</sup> Figure 3 illustrates the EIS Nyquist plots (measured and fitted) for C-steel in 1.0 M HCl without and with different concentrations of PESA and PESAPAM at 25 °C. It can be seen from plots (a) and (b) in Figure 3 that the diameter of the semicircles increases remarkably with the inhibitor concentration. Improved results at higher concentrations demonstrate the adsorption of more polymeric molecules onto the C-steel surface and the formation of a dense protective layer, indicating an effective inhibition.<sup>52</sup> However, the PESA inhibitor over the studied concentration

range (25–500  $\text{mg}\cdot\text{L}^{-1}$ ) exhibited a reversed behavior, where impedance has slightly decreased at 500  $\text{mg}\cdot\text{L}^{-1}$ . This phenomenon indicates exceeding the critical concentration, where thermodynamics plays a role in pulling back the adsorbed inhibitor to the solution.<sup>53</sup> All Nyquist fitted plots possess a single capacitive loop, verifying a charge transfer-controlled corrosion of C-steel.<sup>54</sup>

Comparing the EIS spectra, PESAPAM has a much-boosted inhibition performance rather than PESA as shown in Figure 3. This confirms that grafting and adding the PAM to the PESA chain enhance the adsorption ability of PESA.<sup>55</sup> Indeed, PAM, with its structure containing oxygen and nitrogen heteroatoms, provides more adsorption sites and facilitates the electron transfer from these functional groups to the C-steel surface.<sup>40</sup> Nonetheless, the bulky structure of PAM containing many repeating units could be another essential factor for spreading over a larger surface area, thereby providing more coverage and inhibitive efficiency.

Bode diagrams in Figure 3c,d are helpful to understand further the corrosion mechanism from the frequency responses obtained at high frequencies. Bode curves plotted between  $|Z|$  and frequency show increasing impedance values with the concentration. This comes in compliance with the observed Nyquist trends for PESA and PESAPAM. Also, the phase angle reached 54° and 62° for PESA and PESAPAM, respectively. Overall, the increase in these parameters suggests noteworthy retardation in the diffusion of corrosive species by the formed inhibitor films at the surface.<sup>56</sup>

EIS data are obtained from fitting a typical equivalent electric circuit model shown in Figure 4. For fitting a nonideal double layer capacitor, the circuit components comprise  $R_s$  the solution resistance,  $R_{ct}$  the charge transfer resistance, and CPE a constant phase element.<sup>57</sup>

The CPE impedance is defined according to the following expression:

$$Z_{\text{CPE}} = (Y_0^{-1}(j\omega)^{-n}) \quad (1)$$

where  $Z_{\text{CPE}}$  is CPE impedance in  $\Omega \cdot \text{cm}^{-2}$ ,  $Y_0$  is CPE constant in  $\mu\text{s}^n \cdot \Omega^{-1} \cdot \text{cm}^{-2}$ ,  $j = (-1)^{1/2}$  and  $\omega$  is angular frequency in  $\text{rad} \cdot \text{s}^{-1}$  and  $n$  are the measure to surface inhomogeneity ranging from 0 to 1. The capacitance of the double layer ( $C_{dl}$ ) is calculated based on the charge transfer resistance as follows:

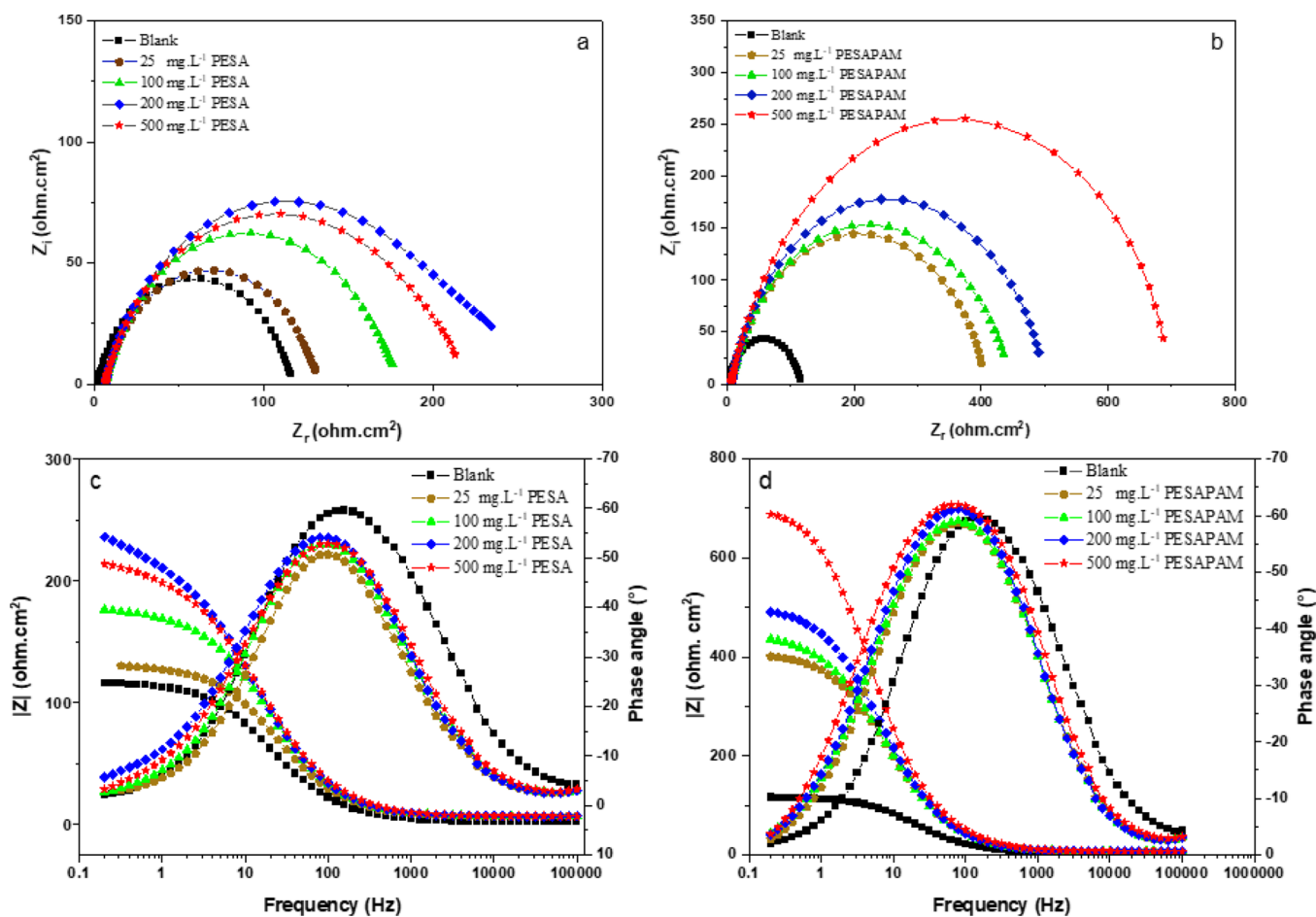


**Figure 3.** Nyquist (a, b) and Bode (c, d) plots of C-steel in 1.0 M HCl without and with different concentrations of PESA and PESAPAM inhibitors.

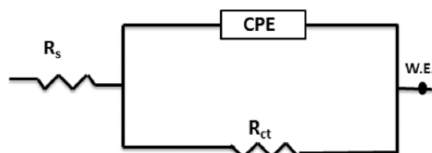


**Figure 4.** Equivalent circuit model for EIS data fitting.

$$C_{dl} = \frac{(Y_0 R_{ct})^{1/n}}{R_{ct}} \quad (2)$$

Then, inhibition efficiency (IE%) can be estimated from  $R_{ct}$  values as:

$$IE\% = \frac{R_{ct1} - R_{ct2}}{R_{ct1}} \times 100 \quad (3)$$

where  $R_{ct1}$  and  $R_{ct2}$  are the charge transfer resistance in the presence and absence of the inhibitor, respectively.

EIS parameters in Table 3 assert the increase in  $R_{ct}$  for the solution containing increasing inhibitor concentrations compared to the uninhibited solution. On the other hand, the formation of a thick double layer with the adsorption of more

**Table 3.** Fitted EIS Measurements and Corrosion Inhibition Efficiencies of PESA and PESAPAM Inhibitors for C-Steel in 1.0 M HCl at 25 °C Obtained from an Equivalent Circuit Model

	inhibitor concentration (mg·L <sup>-1</sup> )	$R_{CT}$ (Ω·cm <sup>2</sup> )	$R_s$ (Ω·cm <sup>2</sup> )	CPE			IE%
				$Y_0$ (μs <sup>n</sup> ·Ω <sup>-1</sup> ·cm <sup>-2</sup> )	$n$	$C_{dl}$ (μF)	
blank	0	116	1.19	236	0.81	218	
PESA	25	125	6.67	186	0.81	78.8	7
	100	171	6.67	177	0.80	75.0	32
	200	222	6.54	199	0.79	85.9	48
	500	202	6.48	189	0.78	76.0	43
PESAPAM	25	400	6.92	134	0.81	65.9	71
	100	431	6.87	140	0.80	69.7	73
	200	488	6.72	125	0.82	66.5	76
	500	700	6.64	116	0.81	63.4	83

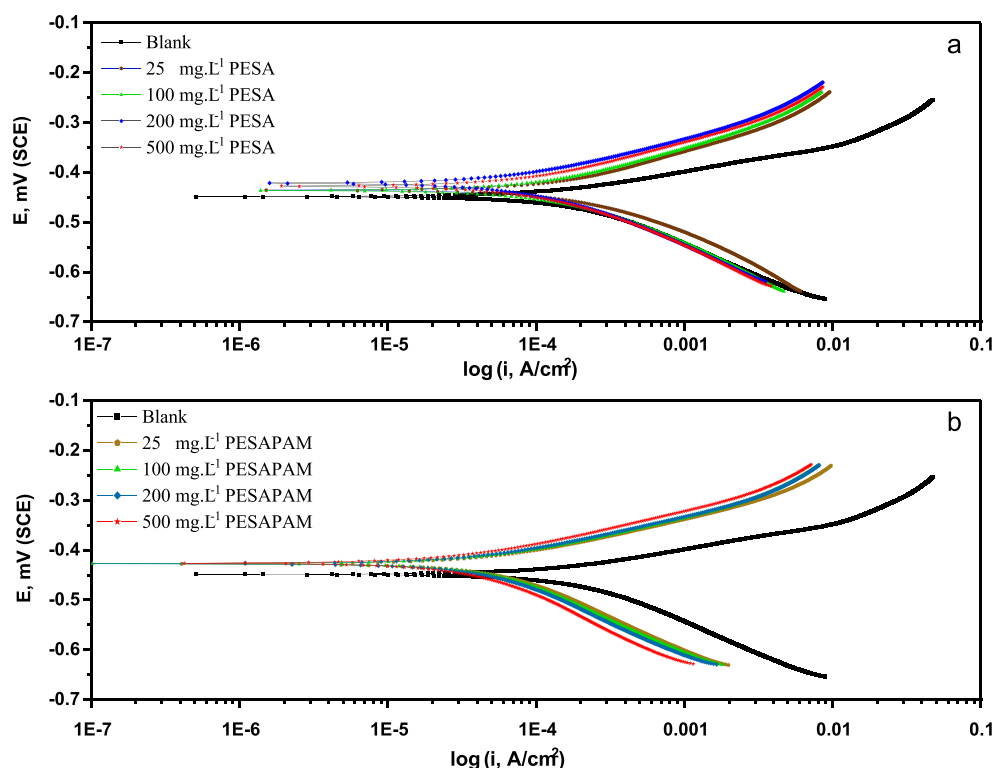


Figure 5. Potentiodynamic polarization curves of C-steel in 1.0 M HCl at different (a) PESA and (b) PESAPAM concentrations.

Table 4. Potentiodynamic Parameters and Corrosion Inhibition Efficiencies of PESA and PESAPAM Inhibitors for C-Steel in 1.0 M HCl at 25 °C Obtained from the Tafel Extrapolation Method

	inhibitor concentration (mg·L <sup>-1</sup> )	$-E_{\text{corr}}$ (mV)	$i_{\text{corr}}$ ( $\mu\text{A}\cdot\text{cm}^{-2}$ )	$\beta_a$ (mV/decade)	$\beta_c$ (mV/decade)	$R_p$ ( $\Omega\cdot\text{cm}^2$ )	CR (mpy)	IE%
blank	0	448	155	61.0	112.7	1.1E-04	70.9	-
PESA	25	436	144	85.6	86.4	4.2E-04	65.9	7
	100	436	106	82.1	93.6	4.5E-04	48.4	32
	200	422	63.1	71.8	84.3	4.9E-04	28.8	59
	500	428	88.7	83.9	99.8	6.1E-04	40.5	43
PESAPAM	25	428	42.6	60.5	129.1	1.3E-04	19.5	73
	100	427	22.9	41.9	54.1	1.8E-04	10.5	85
	200	427	20.6	41.3	53.0	2.7E-04	9.4	87
	500	426	15.6	39.0	50.7	2.2E-04	7.1	90

PESA and PESAPAM molecules onto the surface is confirmed by the reduced  $C_{\text{dl}}$  values at higher concentrations.<sup>11</sup> It is constantly recognized that the ideal inhibitor performance is considered at the highest  $R_{\text{ct}}$  and the lowest  $C_{\text{dl}}$  values obtained.<sup>58</sup> The tabulated measurements give evidence that PESAPAM exhibits much more efficient inhibition performance than PESA alone. The charge transfer resistance reached the maximum of 700 and 222  $\Omega\cdot\text{cm}^2$  for PESAPAM and PESA, respectively. Therefore, EIS tests reveal a substantial inhibition efficiency improvement of around 40%, reaching 83% with the addition of the grafted PESA polymer (PESAPAM). As explained earlier, the efficiency of the PESA inhibitor has slightly decreased from 48 to 43% upon exceeding the critical concentration of 200 mg·L<sup>-1</sup>. It is worth mentioning that even at a low concentration of 25 mg·L<sup>-1</sup>, PESAPAM has a pronounced effect on inhibiting the corrosion of C-steel in 1.0 M HCl by 71%. These results will impact positively the economy cost when using large quantities of the inhibitor in large water carriers where PESAPAM can reach higher efficiency than PESA.

### 3.4. Potentiodynamic Polarization Measurements.

Potentiodynamic polarization tests of C-steel in 1.0 M HCl in the absence and presence of PESA and PESAPAM inhibitors were performed at 25 °C. These tests were examined to elucidate the corrosion kinetics of the anodic and cathodic reactions. Figure 5 clearly shows a shift of anodic and cathodic branches toward less negative values after adding PESA and PESAPAM, maintaining the same general curve shape. However, the estimated negative shift of both branches is less than 85 mV, indicating both polymers act as mixed-type inhibitors.<sup>59,60</sup>

Indeed, curves in Figure 5b exhibited a larger shift from the HCl blank curve compared to the shifts in Figure 5a. This also implies that PESAPAM behaves as a better corrosion inhibitor than PESA. The superior performance of PESAPAM could additionally be attributed to the strong interaction of the positively charged protonated species with the negatively charged metallic surface with Cl<sup>-</sup> adsorbed.<sup>61</sup> It was stated that there is a possible protonation of PAM at the oxygen which creates resonance stabilization of positive charges, thereby

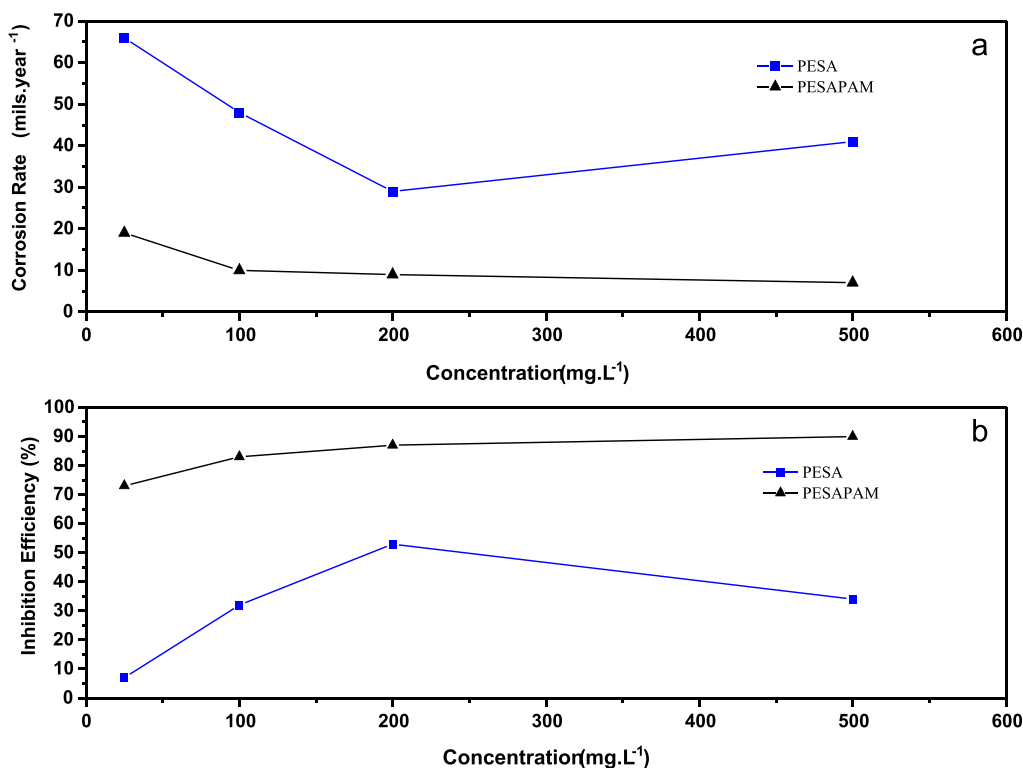


Figure 6. Effect of PESA and PESAPAM concentrations on (a) corrosion rate and (b) inhibition efficiency.

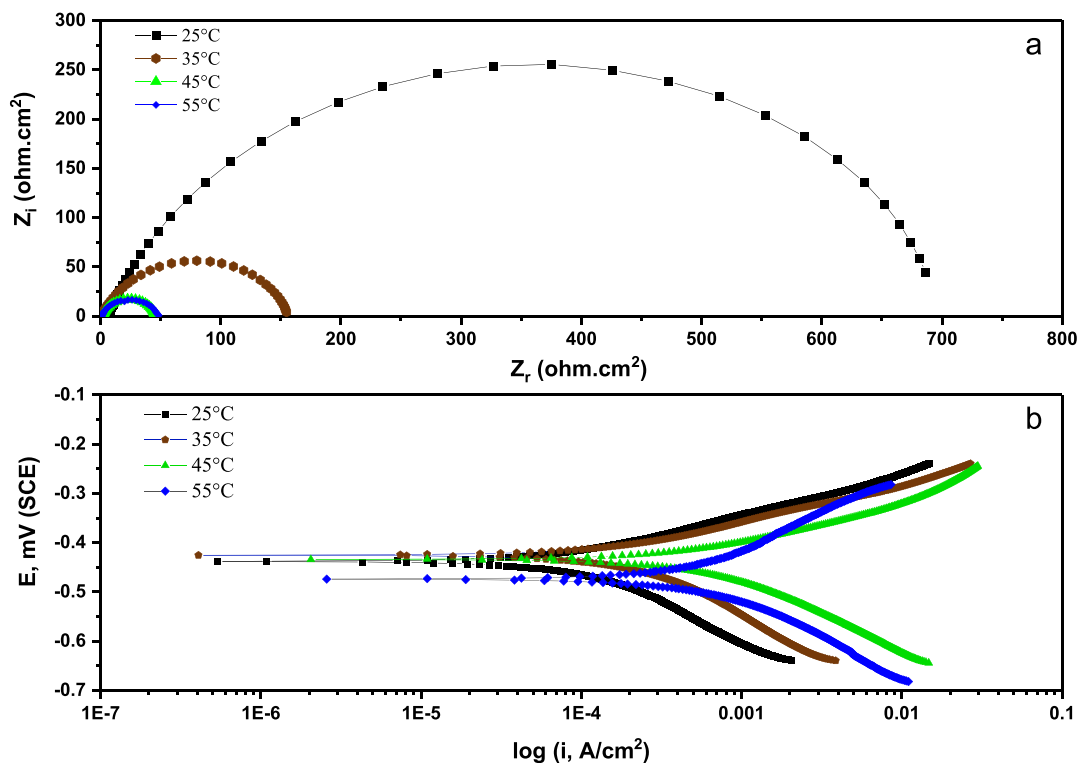


Figure 7. Effect of temperature on (a) EIS and (b) potentiodynamic polarization curves for C-steel in 1.0 M HCl in the presence of 500 mg.L<sup>-1</sup> PESAPAM.

facilitating the adsorption of PESAPAM onto the steel surface.<sup>40</sup>

Furthermore, the curves shift toward lower current densities at higher inhibitor concentrations. Consequently, cathodic hydrogen evolution and anodic metallic dissolution are both

retarded by the addition of inhibitors. The visual examination of both graphs in Figure 5 affirms that cathodic curves are considerably altered to lower current densities by adding different concentrations of PESAPAM rather than PESA. Therefore, PESAPAM has the predominant potential to cover

the active cathodic sites at all studied concentrations. This confirms that the reduced availability of active sites in the case of adding a PESAPAM inhibitor could substantially decelerate the rate of hydrogen evolution reactions, corresponding to the much lower current densities observed in Figure 5b compared to Figure 5a.<sup>62</sup>

The potential potentiodynamic corrosion parameters were obtained by the Tafel extrapolation method. Electrochemical parameters comprising the free potential ( $E_{\text{corr}}$ ), current density ( $i_{\text{corr}}$ ), polarization resistance ( $R_p$ ), corrosion rate (CR), and anodic ( $\beta_a$ ) and cathodic ( $\beta_c$ ) slopes of Tafel branches are tabulated in Table 4.

The Stern–Geary equation was followed to determine the polarization resistance ( $R_p$ ):

$$R_p = \frac{\beta_a \beta_c}{2.303 i_{\text{corr}} (\beta_a + \beta_c)} \quad (4)$$

IE% is determined from the current density ( $i_{\text{corr}}$ ) as:

$$\text{IE\%} = \frac{i_{\text{corr}1} - i_{\text{corr}2}}{i_{\text{corr}1}} \times 100 \quad (5)$$

where  $i_{\text{corr}1}$  and  $i_{\text{corr}2}$  are the corrosion current densities in the absence and presence of the inhibitor, respectively.

The formation of a protective layer on the C-steel surface in the presence of both inhibitors is fundamentally interpreted by the reduced current densities, CRs, and reinforced polarization resistance.<sup>63,64</sup> Higher concentrations of both inhibitors have successfully weakened the adsorption affinity of C-steel toward chloride ions, thus lowering the CRs, as in Figure 6. Furthermore, comparing the current densities of both inhibitors revealed a decrease from 88.7  $\mu\text{A}\cdot\text{cm}^{-2}$  in the case of PESA to 15.6  $\mu\text{A}\cdot\text{cm}^{-2}$  for the PESAPAM. The significant reduction in current densities could be ascribed to the boosted electron density over the C-steel surface, where an excessive accumulation of molecules at higher inhibitor concentrations occurs, resulting in an inhibiting film.

The PESA inhibitor has noticeably reduced the CR of C-steel by 43%, from 71 mils per year in the blank solution to a minimum of 40.5 mils per year in the presence of 500  $\text{mg}\cdot\text{L}^{-1}$  inhibitor (Figure 6a). However, grafting PAM onto the PESA chains influences the PESAPAM inhibitor to remarkably diminish the corrosion rate to 7.1 mils per year at 500  $\text{mg}\cdot\text{L}^{-1}$ , resulting in a 90% reduction in the overall corrosion rate. Despite that, PESAPAM succeeded in reaching 90% inhibition efficiency at the highest tested concentration of 500  $\text{mg}\cdot\text{L}^{-1}$ , as shown in Figure 6b. This displays an overall improvement of PESA efficiency that reached 43% by approximately 109% at the same concentration.

**3.5. Temperature Effect.** The above-discussed electrochemical measurements have disclosed a predominant performance for PESAPAM. Therefore, the effectiveness of this synthesized PESAPAM inhibitor was further investigated at variable temperature. The potentiodynamic curves for C-steel in the presence of 500  $\text{mg}\cdot\text{L}^{-1}$  PESAPAM at temperatures of 25, 35, 45, and 55 °C are shown in Figure 7. It is observed that the performance of PESAPAM has deteriorated, with depressed semicircles during the temperature rise.<sup>65</sup> The identical shape of semicircles explains a maintained acidic corrosion mechanism, however, with altered dielectric properties of the electric double layer by the added inhibitor.<sup>66</sup> Furthermore, the potentiodynamic curves shift toward more negative potentials and higher current densities.<sup>67</sup>

The electrochemical parameters of PESAPAM at different temperatures in the range of 25–55 °C are all listed in Tables 5 and 6. EIS results show that the charge transfer is reduced by

**Table 5. Effect of Temperature on Fitted EIS Measurements of the PESAPAM Inhibitor for C-Steel in 1.0 M HCl**

temperature (°C)	$R_{\text{CT}}$ ( $\Omega\cdot\text{cm}^2$ )	$R_s$ ( $\Omega\cdot\text{cm}^2$ )	$Y_0$ ( $\mu\text{s}^n\cdot\Omega^{-1}\cdot\text{cm}^{-2}$ )	$n$	$C_{\text{dl}}$ ( $\mu\text{F}$ )
25	700.0	6.6	1.2E-04	0.81	6.7E-05
35	158.7	0.9	2.6E-04	0.77	1.0E-04
45	44.5	1.8	2.2E-04	0.82	7.7E-05
55	47.7	1.0	7.6E-04	0.78	3.0E-04

93% from 700 to 47.7  $\Omega\cdot\text{cm}^2$  as a consequence of the overall 30 °C temperature increase. In addition, the temperature influences a gradual rise in the double layer capacitance  $C_{\text{dl}}$ .<sup>68</sup>

Moreover, the potentiodynamic parameters in Table 6 present the CR increase with the temperature rise. The presence of 500  $\text{mg}\cdot\text{L}^{-1}$  PESAPAM has a hindered corrosion protection capability at higher temperatures due to the elevation in the inhibitor desorption rate from the C-steel surface.<sup>69</sup> The CR was approximately 32 times higher at 55 °C than at 25 °C, reaching 288 mils per year. Additionally, current density dramatically increases with the temperature rise. The current density is increased from 21 to 632  $\mu\text{A}\cdot\text{cm}^{-2}$ , which could be ascribed to the accelerated metal dissolution and inability of the polymer to form a protective film at higher temperatures.<sup>70</sup>

Temperature variations are definitely associated with a change in the rate of chemical reactions. Determining corrosion kinetic parameters is critical to clarify the dissolution behavior of the C-steel surface. Therefore, the activation energy ( $E_a$ ), enthalpy ( $\Delta H_a$ ), and entropy ( $\Delta S_a$ ) of activation are all calculated from the below Arrhenius equation.

$$\log(\text{CR}) = \frac{-E_a}{2.303 RT} \quad (6)$$

where CR is the corrosion rate,  $E_a$  is the activation energy,  $R$  is the universal gas constant in  $\text{J}\cdot\text{mol}^{-1}\cdot\text{K}^{-1}$ , and  $T$  is the temperature in K.

The slope of Figure 8 plotted for  $\log(\text{CR})$  versus  $1/T$  estimates an activation energy  $E_a$  value of 85.3  $\text{kJ}\cdot\text{mol}^{-1}$ , which interprets physical adsorption.<sup>71</sup> Different studies also showed physical adsorption of cefazolin and pyridinium ionic liquid at activation energies of 89 and 84.7  $\text{kJ}\cdot\text{mol}^{-1}$ , respectively.<sup>71,72</sup>

The transition-state equation, an alternative form of the Arrhenius equation, was followed to calculate the  $\Delta H_a$  and  $\Delta S_a$ .

$$\text{CR} = \frac{RT}{Nh} e^{\Delta S_a^*/R} e^{-\Delta H_a^*/RT} \quad (7)$$

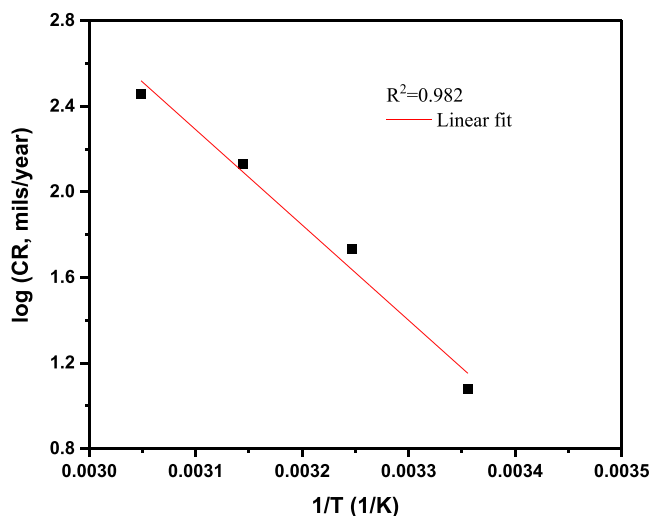
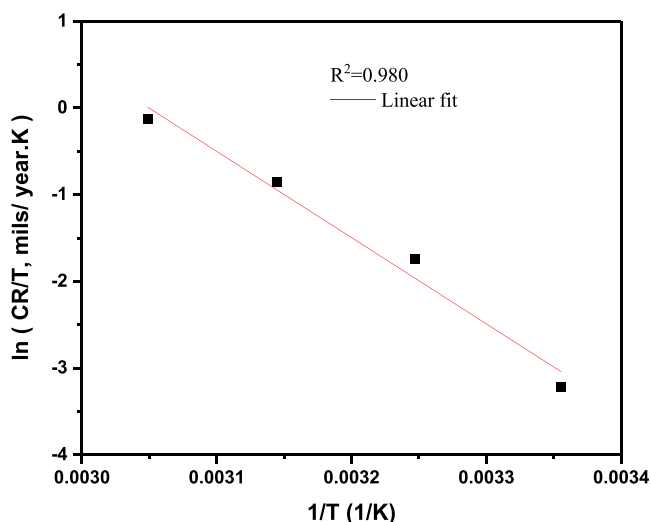
where CR is the corrosion rate,  $N$  is the Avogadro number,  $h$  is the Planck constant,  $E_a$  is the activation energy,  $\Delta H_a$  is the activation enthalpy in  $\text{kJ}\cdot\text{mol}^{-1}$  and  $\Delta S_a$  is the activation entropy in  $\text{J}\cdot\text{mol}^{-1}\cdot\text{K}^{-1}$ ,  $R$  is the universal gas constant in  $\text{J}\cdot\text{mol}^{-1}\cdot\text{K}^{-1}$ , and  $T$  is the temperature in K.

A plot of  $\ln(\text{CR}/T)$  versus  $1/T$  in Figure 9 is used to determine the values of  $\Delta H_a$  and  $\Delta S_a$  from the slope and intercept, respectively. Results show values of 83  $\text{kJ}\cdot\text{mol}^{-1}$  for  $\Delta H_a$  and 274  $\text{J}\cdot\text{mol}^{-1}$  for  $\Delta S_a$ . The dissolution of C-steel is



**Table 6. Effect of Temperature on Fitted Potentiodynamic Parameters of the PESAPAM Inhibitor for C-Steel in 1.0 M HCl**

temperature (°C)	$-E_{\text{corr}}$ (mV)	$i_{\text{corr}}$ ( $\mu\text{A}\cdot\text{cm}^{-2}$ )	$\beta_a$ (mV/decade)	$\beta_c$ (mV/decade)	$R_p$ ( $\Omega\cdot\text{cm}^2$ )	CR (mpy)
25	-438	21	30.8	30.8	3.2E-04	12
35	-425	120	62.8	86.5	1.3E-04	54
45	-434	315	62.9	71.9	4.8E-05	144
55	-474	632	192.3	129.7	5.3E-05	288

**Figure 8.** Arrhenius plot of  $\log(\text{CR})$  versus  $1/T$  for C-steel in 1.0 M HCl with  $500\text{ mg}\cdot\text{L}^{-1}$  PESAPAM at different temperatures.**Figure 9.** Transition-state plots of  $\log(\text{CR}/T)$  versus  $(1/T)$  for C-steel in 1.0 M HCl with  $500\text{ mg}\cdot\text{L}^{-1}$  PESAPAM at different temperatures.

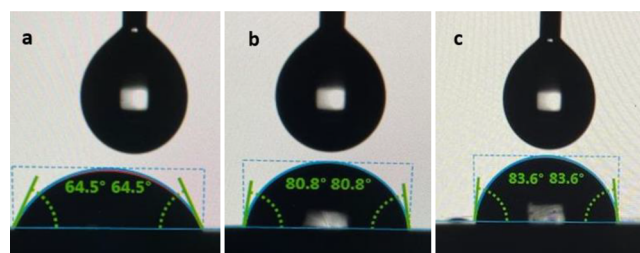
endothermic, and the presence of the inhibitor increases the disorder, as denoted by the positive values of  $\Delta H_a$  and  $\Delta S_a$ . This suggests that the system disorder could be influenced by replacing water molecules with the PESAPAM large polymeric molecules adsorbing irregularly onto the C-steel surface.<sup>73</sup> The present conditions express a unimolecular corrosion process as the difference of  $E_a - \Delta H_a$  (Table 7) is almost comparable to the average value of  $RT$ .<sup>72</sup>

**3.6. Contact Angle Measurements.** In order to obtain more insight into the mechanism of corrosion inhibition, the hydrophobic and hydrophilic characteristics of the C-steel surface were analyzed using contact angle measurements. The

**Table 7. Corrosion Kinetic Parameters for C-Steel in 1.0 M HCl in the Presence of  $500\text{ mg}\cdot\text{L}^{-1}$  PESAPAM**

$E_a$ ( $\text{kJ}\cdot\text{mol}^{-1}$ )	85.3
$\Delta H_a$ ( $\text{kJ}\cdot\text{mol}^{-1}$ )	83
$\Delta S_a$ ( $\text{J}\cdot\text{mol}^{-1}$ )	274

steel samples were immersed in 1.0 M HCl solution without and with  $500\text{ mg}\cdot\text{L}^{-1}$  PESA and PESAPAM polymeric inhibitors for 6 h at  $25\text{ }^\circ\text{C}$ . Ten measurements were carried out at different spots, and average values were reported for each testing condition (Figure 10). Each contact angle

**Figure 10.** Contact angle measurements of C-steel in 1.0 M HCl in the absence (a) and presence of  $500\text{ mg}\cdot\text{L}^{-1}$  (b) PESA and (c) PESAPAM inhibitors after immersion of 6 h at  $25\text{ }^\circ\text{C}$ .

measurement was attained by depositing a  $10\text{ }\mu\text{L}$  water droplet on the C-steel surface. The average contact angle of examined C-steel after corrosion in the blank solution is  $65.5^\circ$  with a standard deviation of 2.8 (Figure 10a). However, the average contact angles of C-steel after corrosion with PESA and PESAPAM inhibitors increased to  $80.0^\circ$  and  $84.2^\circ$  with a standard deviation of 0.7 and 1, respectively (Figure 10b,c). Elevation in contact angle measurements confirms the adsorption of both inhibitors onto the C-steel and further explains the improvement in corrosion performance by increasing surface hydrophobicity and hence repelling water from the surface.

**3.7. Morphological Analyses.** **3.7.1. Scanning Electron Microscopy (SEM).** The surface morphology of C-steel before and after immersion in 1.0 M HCl with the absence and presence of  $500\text{ mg}\cdot\text{L}^{-1}$  PESA and PESAPAM inhibitors for 6 h at  $25\text{ }^\circ\text{C}$  is shown in Figure 11. The C-steel surface (Figure 11a) before corrosion experiments shows a generally smooth surface, with no significant defects with a slightly rough surface due to scratches that emerged during the polishing stage. In contrast, a highly corroded and damaged surface is observed in Figure 11b, with several deep and wide pits with secondary pitting observed as marked in the SEM micrograph, due to the destructive immersion in the blank HCl solution. In addition to that, adding PESA and PESAPAM inhibitors proved their capabilities in protecting the surface and retarding the corrosion relying on SEM micrographs in Figure 11c,d as indicative by the formation of a dense film. The steel specimen immersed in the PESA inhibitor shows the formation of a

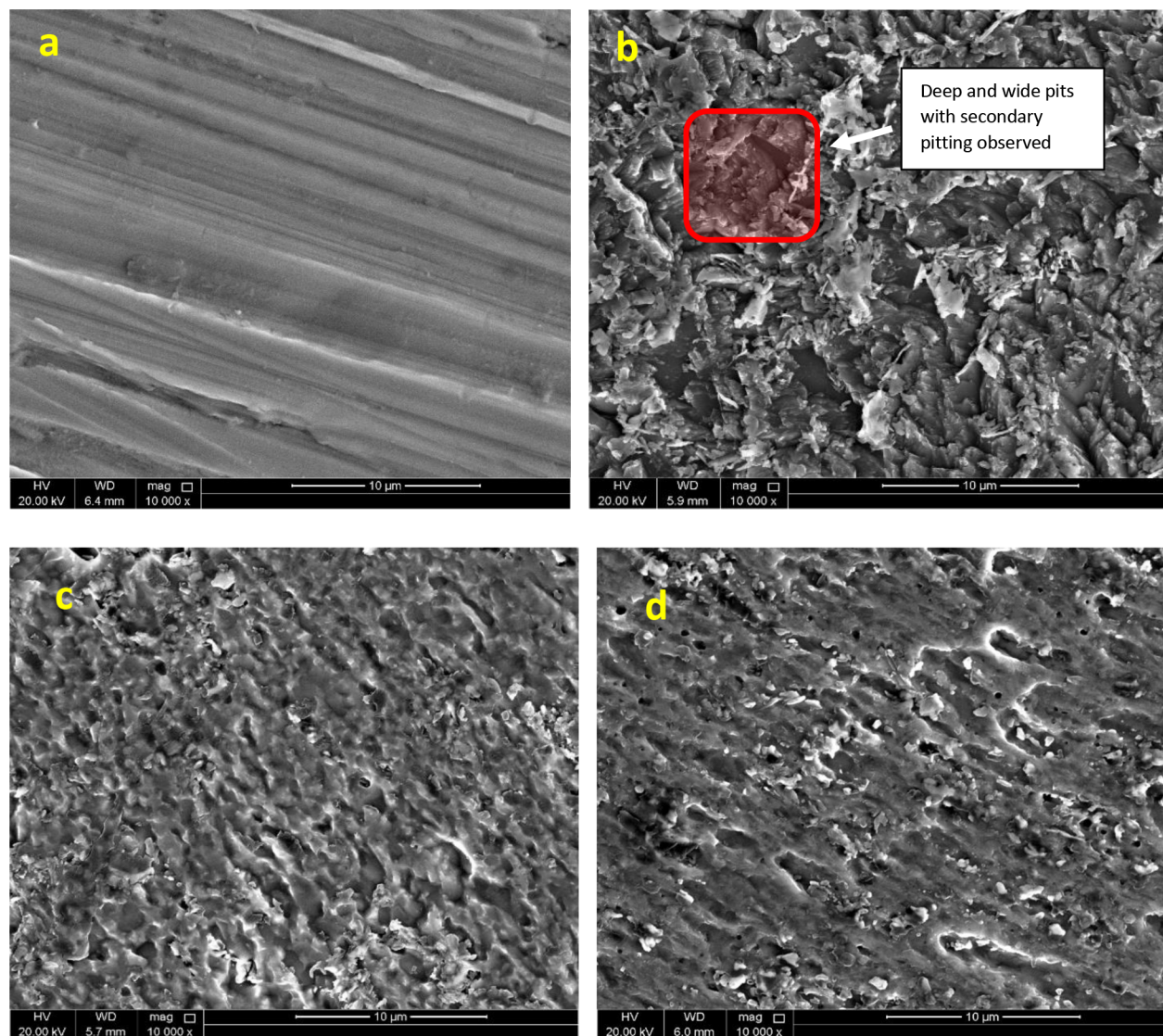


**Figure 11.** SEM micrographs of (a) polished C-steel (b) in 1.0 M HCl, and in the presence of 500 mg·L<sup>-1</sup> (c) PESA and (d) PESAPAM after immersion of 6 h at 25 °C.

dense protective layer with scattered small pits. The specimen immersed in PESAPAM exhibited more homogeneous and flat areas, with lower roughness indicating an improved corrosion protection compared to PESA alone. Consequently, the investigated morphology analysis complies with the electrochemical measurements, confirming a superior protective film formation by PESAPAM onto the C-steel surface.<sup>74</sup>

**3.7.2. Energy-Dispersive X-ray (EDX) Analysis.** The EDX technique was employed to understand the chemical components formed on the C-steel surface during the corrosion process in the absence and presence of both PESA and PESAPAM inhibitors. EDX spectra of polished, uninhibited, and inhibited specimens immersed for 6 h in solutions are demonstrated in Figure 12, with the peaks of corresponding elements.

The atomic component percentages found in C-steel before and after immersion in a blank 1.0 M HCl corrosive medium are (2.61% C and 97.39% Fe) and (88.57% Fe, 5.02% C, and 6.40% O). The detected components indicate the development of an iron oxide layer on the corroded C-steel surface. Adding 500 mg·L<sup>-1</sup> PESA inhibitor reveals component percentages of

94.22% Fe, 4.45% C, and 1.32% O, indicating reduced oxide layer formation. Correspondingly, the acquired components for the inhibited solution with 500 mg·L<sup>-1</sup> PESAPAM display 92.53% Fe, 5.14% C, 1.73% O, and 0.6% N. The detected nitrogen element on the C-steel surface after immersion in PESAPAM provides evidence of the amine group adsorption in the PAM structure. Consequently, the outcomes of the EDX spectra are consistent with all experimental measurements, confirming the reduction in corrosion and protection of the C-steel surface by the adsorbed polymeric inhibitors.<sup>75</sup> It is also elucidated that a better inhibitive polymer film is formed by PESAPAM, where an increase in the atomic carbon % was observed, representing the bulky organic polymer existence.

#### 4. CONCLUSIONS

Developing effective CIs is necessary to protect industrial materials and lower economic losses. Lately, environmentally friendly inhibitors have been attracting attention to resolve the environmental problems associated with the injection of these compounds. The principal aim of this research study is to investigate the performance of novel PESA-grafted PAM

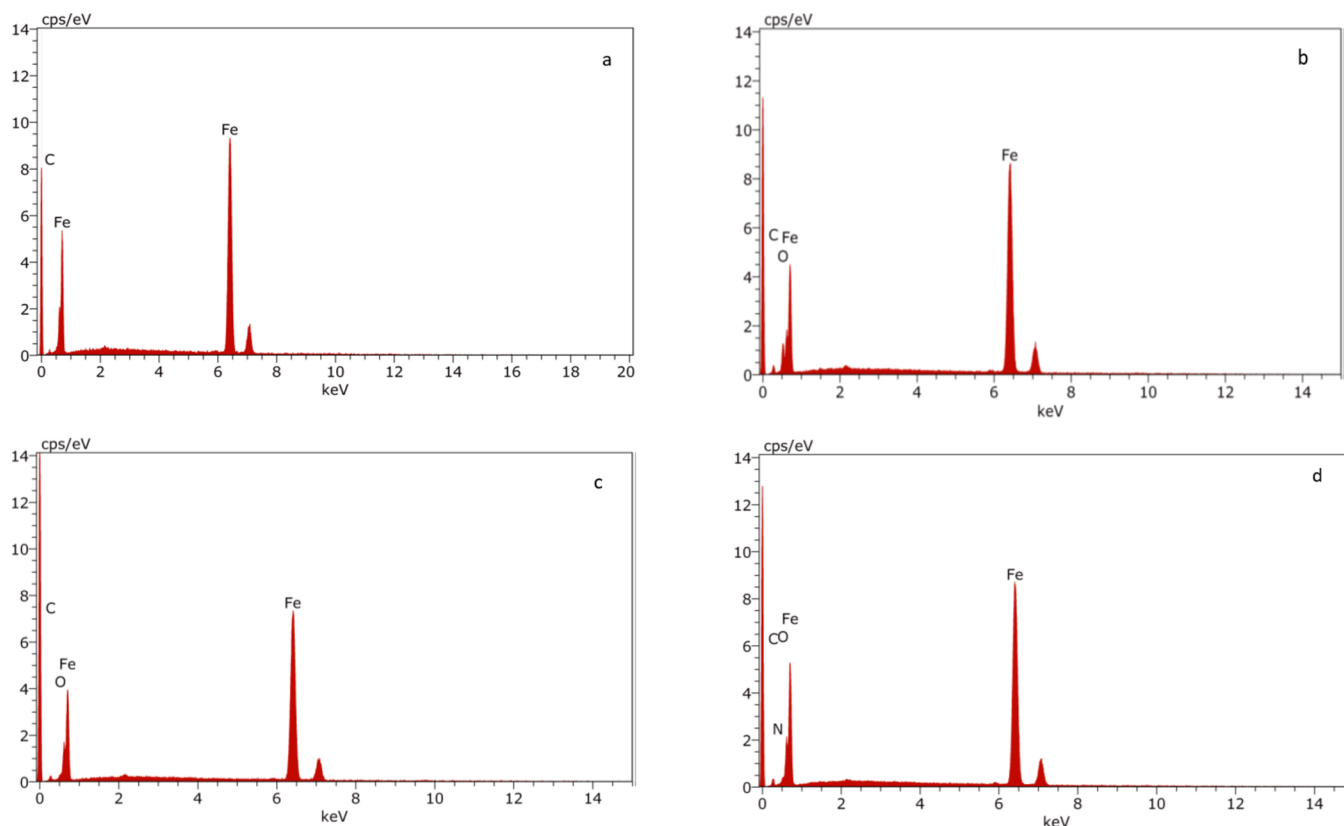


**Figure 12.** EDX spectra of (a) polished C-steel before immersion in 1.0 M HCl in the absence (b) and presence of 500 mg·L<sup>-1</sup> (c) PESA and (d) PESAPAM for 6 h at 25 °C.

(PESAPAM) on C-steel corrosion in 1.0 M HCl. The following conclusions are obtained:

1. PESAPAM exhibited extraordinary corrosion inhibition with the concentration increase and achieved 90% efficiency at 500 mg·L<sup>-1</sup> concentration.
2. The comparative analysis revealed a remarkable enhancement of PESA inhibitive performance after PAM grafting, considering an efficiency improvement from 7 to 73%, even in the presence of a low concentration of 25 mg·L<sup>-1</sup> in 1.0 M HCl.
3. Electrochemical impedance investigation confirmed the formation of a thick double layer with the adsorption of PESAPAM molecules onto the C-steel surface.
4. The potentiodynamic study discloses both PESA and PESAPAM polymers as mixed-type inhibitors.
5. A corrosion kinetics study at elevated temperatures predicts a physical adsorption nature of PESAPAM on the C-steel surface.
6. The increased surface hydrophobicity also indicates the desired adsorption of PESAPAM on steel, relying on contact angle measurements.
7. SEM and EDX surface characterizations of steel specimens proved the formation of a protective film on the metal surface and revealed reduced damage of corrosion attack.

## ■ AUTHOR INFORMATION

### Corresponding Authors

Mazen Khaled – Department of Chemistry and Earth Sciences, College of Arts and Sciences, Qatar University, Doha 974,

Qatar; [orcid.org/0000-0002-8826-2413](https://orcid.org/0000-0002-8826-2413); Phone: +974 4403 4672/7694; Email: [mkhaled@qu.edu.qa](mailto:mkhaled@qu.edu.qa)

Ibnelwaleed A. Hussein – Gas Processing Center, College of Engineering and Chemical Engineering Department, College of Engineering, Qatar University, Doha 974, Qatar;

[orcid.org/0000-0002-6672-8649](https://orcid.org/0000-0002-6672-8649); Phone: +974 4403 7694; Email: [ihussein@qu.edu.qa](mailto:ihussein@qu.edu.qa)

### Authors

Rem Jalab – Gas Processing Center, College of Engineering, Qatar University, Doha 974, Qatar

Ahmed Ben Ali – Gas Processing Center, College of Engineering, Qatar University, Doha 974, Qatar

Maha Abouseada – Department of Chemistry and Earth Sciences, College of Arts and Sciences, Qatar University, Doha 974, Qatar

Safa AlKhalil – Department of Chemistry and Earth Sciences, College of Arts and Sciences, Qatar University, Doha 974, Qatar

Amna Al-Suwaidi – Chemical Engineering Department, College of Engineering, Qatar University, Doha 974, Qatar

Sali Hamze – Chemical Engineering Department, College of Engineering, Qatar University, Doha 974, Qatar

Complete contact information is available at:

<https://pubs.acs.org/10.1021/acsomega.2c07607>

### Notes

The authors declare no competing financial interest.

## ACKNOWLEDGMENTS

This work was made possible by the support of the Undergraduate Research Experience Program (UREP) from Qatar National Research Fund (QNRF), grant #UREP28-104-2-036. R.J. would like to acknowledge the support of Qatar University project, grant #QUCP-CENG-2021-03. The findings achieved herein are solely the responsibility of the authors. Central Laboratories Unit at Qatar University are acknowledged for providing facilities to perform SEM/EDX analyses. Qatar National Library (QNL) is acknowledged for providing open access funding.

## REFERENCES

- (1) Dwivedi, D.; Lepková, K.; Becker, T. Carbon Steel Corrosion: A Review of Key Surface Properties and Characterization Methods. *RSC Adv.* **2017**, *7*, 4580–4610.
- (2) Raj, R.; Morozov, Y.; Calado, L. M.; Taryba, M. G.; Kahraman, R.; Shakoor, A.; Montemor, M. F. Inhibitor Loaded Calcium Carbonate Microparticles for Corrosion Protection of Epoxy-Coated Carbon Steel. *Electrochim. Acta* **2019**, *319*, 801–812.
- (3) Kahyarian, A.; Schumaker, A.; Brown, B.; Nestic, S. Acidic Corrosion of Mild Steel in the Presence of Acetic Acid: Mechanism and Prediction. *Electrochim. Acta* **2017**, *258*, 639–652.
- (4) Sadeghi Erami, R.; Amirnasr, M.; Meghdadi, S.; Talebian, M.; Farrokhpour, H.; Raeissi, K. Carboxamide Derivatives as New Corrosion Inhibitors for Mild Steel Protection in Hydrochloric Acid Solution. *Corros. Sci.* **2019**, *151*, 190–197.
- (5) Abdallah, M.; Altass, H. M.; Al-Gorair, A. S.; Al-Fahemi, J. H.; Jahdaly, B. A. A. L.; Soliman, K. A. Natural Nutmeg Oil as a Green Corrosion Inhibitor for Carbon Steel in 1.0 M HCl Solution: Chemical, Electrochemical, and Computational Methods. *J. Mol. Liq.* **2021**, *323*, No. 115036.
- (6) Verma, C.; Ebenso, E. E.; Quraishi, M. A.; Hussain, C. M. Recent Developments in Sustainable Corrosion Inhibitors: Design, Performance and Industrial Scale Applications. *Mater. Adv.* **2021**, *2*, 3806–3850.
- (7) Renner, F. U.; Stierle, A.; Dosch, H.; Kolb, D. M.; Lee, T. L.; Zegenhagen, J. Initial Corrosion Observed on the Atomic Scale. *Nature* **2006**, *439*, 707–710.
- (8) Tamalmani, K.; Husin, H. Review on Corrosion Inhibitors for Oil and Gas Corrosion Issues. *Appl. Sci.* **2020**, *10*, 3389.
- (9) Umoren, S. A.; Solomon, M. M.; Saji, V. S. Corrosion Inhibitors for Sour Oilfield Environment (H<sub>2</sub>S Corrosion). In *Corrosion Inhibitors in the Oil and Gas Industry*; Saji, V. S., Umoren, S. A., Eds.; Wiley-VCH Verlag GmbH & Co. KGaA, 2020; Vol. 2020, pp 229–254.
- (10) Hou, B.; Li, X.; Ma, X.; Du, C.; Zhang, D.; Zheng, M.; Xu, W.; Lu, D.; Ma, F. The Cost of Corrosion in China. *npj Mater. Degrad.* **2017**, *1*, 4.
- (11) Zeino, A.; Abdulazeez, I.; Khaled, M.; Jawish, M. W.; Obot, I. B.; Alhooshani, K. Mechanistic Study of Polyepoxy Succinic Acid (PESA) as Green Corrosion Inhibitor on Carbon Steel in Aerated NaCl Solution. *Mater. Today Commun.* **2021**, *29*, No. 102848.
- (12) Prabakaran, M.; Durainatarajan, P.; Ramesh, S.; Periasamy, V. Enhanced Corrosion Inhibition Behavior of Carbon Steel in Aqueous Solution by Phosphoserine-Zn<sup>2+</sup> System. *J. Adhes. Sci. Technol.* **2016**, *30*, 1487–1509.
- (13) Farhadian, A.; Varfolomeev, M. A.; Kudbanov, A.; Rezaeisadat, M.; Nurgaliev, D. K. Waterborne Polymers as Kinetic/Anti-Agglomerant Methane Hydrate and Corrosion Inhibitors: A New and Promising Strategy for Flow Assurance. *J. Nat. Gas Sci. Eng.* **2020**, *77*, No. 103235.
- (14) Verma, C.; Olasunkanmi, L. O.; Quadri, T. W.; Sherif, E. S. M.; Ebenso, E. E. Gravimetric, Electrochemical, Surface Morphology, DFT, and Monte Carlo Simulation Studies on Three N-Substituted 2-Aminopyridine Derivatives as Corrosion Inhibitors of Mild Steel in Acidic Medium. *J. Phys. Chem. C* **2018**, *122*, 11870–11882.
- (15) Arthur, D. E.; Jonathan, A.; Ameh, P. O.; Anya, C. A Review on the Assessment of Polymeric Materials Used as Corrosion Inhibitor of Metals and Alloys. *Int. J. Ind. Chem.* **2013**, *4*, 2.
- (16) Verma, C.; Quraishi, M. A.; Rhee, K. Y. Aqueous Phase Polymeric Corrosion Inhibitors: Recent Advancements and Future Opportunities. *J. Mol. Liq.* **2022**, *348*, No. 118387.
- (17) Dong, J.; Pan, W.; Luo, J.; Liu, R. Synthesis of Inhibitor-Loaded Polyaniline Microcapsules with Dual Anti-Corrosion Functions for Protection of Carbon Steel. *Electrochim. Acta* **2020**, *364*, No. 137299.
- (18) Beniken, M.; Salim, R.; Ech-chihbi, E.; Sfaira, M.; Hammouti, B.; Ebn Touhami, M.; Mohsin, M. A.; Taleb, M. Adsorption Behavior and Corrosion Inhibition Mechanism of a Polyacrylamide on C–Steel in 0.5 M H<sub>2</sub>SO<sub>4</sub>: Electrochemical Assessments and Molecular Dynamic Simulation. *J. Mol. Liq.* **2022**, *348*, No. 118022.
- (19) Nwanonenyi, S. C.; Obasi, H. C.; Chukwujike, I. C.; Chidiebere, M. A.; Oguzie, E. E. Inhibition of Carbon Steel Corrosion in 1 M H<sub>2</sub>SO<sub>4</sub> Using Soy Polymer and Polyvinylpyrrolidone. *Chem. Afr.* **2019**, *2*, 277–289.
- (20) Ouass, A.; Galai, M.; Ouakki, M.; Ech-Chihbi, E.; Kadiri, L.; Hsissou, R.; Essaadaoui, Y.; Berisha, A.; Cherkaoui, M.; Lebkiri, A.; Rifi, E. H. Poly(Sodium Acrylate) and Poly(Acrylic Acid Sodium) as an Eco-Friendly Corrosion Inhibitor of Mild Steel in Normal Hydrochloric Acid: Experimental, Spectroscopic and Theoretical Approach. *J. Appl. Electrochem.* **2021**, *51*, 1009–1032.
- (21) Palaniappan, N.; Cole, I. S.; Kuznetsov, A. E.; Justin Thomas, K. R. Experimental and DFT Studies of Carbon Nanotubes Covalently Functionalized with an Imidazole Derivative for Electrochemical Stability and Green Corrosion Inhibition as a Barrier Layer on the Nickel Alloy Surface in a Sulphuric Acidic Medium. *RSC Adv.* **2019**, *9*, 38677–38686.
- (22) Ituen, E.; Mkpenie, V.; Dan, E. Surface Protection of Steel in Oil Well Acidizing Fluids Using L-Theanine-Based Corrosion Inhibitor Formulations: Experimental and Theoretical Evaluation. *Surf. Interfaces* **2019**, *16*, 29–42.
- (23) Cioc, R. C.; Ruijter, E.; Orru, R. V. A. Multicomponent Reactions: Advanced Tools for Sustainable Organic Synthesis. *Green Chem.* **2014**, *16*, 2958–2975.
- (24) Verma, C.; Quraishi, M. A.; Ebenso, E. E. Microwave and Ultrasound Irradiations for the Synthesis of Environmentally Sustainable Corrosion Inhibitors: An Overview. *Sustainable Chem. Pharm.* **2018**, *10*, 134–147.
- (25) Eduardo, T.; Rita, M.; Vega, O.; Schroeder, R.; Fernandes, S.; Muller, L.; Mattedi, S.; Taryba, M. Localized Corrosion Behavior Studies by SVET of 1010 Steel in Different Concentrations of Sodium Chloride Containing [m-2HEA][Ol] Ionic Liquid as Corrosion Inhibitor. *Electrochim. Acta* **2022**, *419*, No. 140385.
- (26) Boudelloua, H.; Hamlaoui, Y.; Tifouti, L.; Pedraza, F. Effects of Polyethylene Glycol (PEG) on the Corrosion Inhibition of Mild Steel by Cerium Nitrate in Chloride Solution. *Appl. Surf. Sci.* **2019**, *473*, 449–460.
- (27) Ye, Y.; Chen, H.; Zou, Y.; Zhao, H. Study on Self-Healing and Corrosion Resistance Behaviors of Functionalized Carbon Dot-Intercalated Graphene-Based Waterborne Epoxy Coating. *J. Mater. Sci. Technol.* **2021**, *67*, 226–236.
- (28) Zeino, A.; Abdulazeez, I.; Khaled, M.; Jawish, M. W.; Obot, I. B. Mechanistic Study of Polyaspartic Acid (PASP) as Eco-Friendly Corrosion Inhibitor on Mild Steel in 3% NaCl Aerated Solution. *J. Mol. Liq.* **2018**, *250*, 50–62.
- (29) Huang, H.; Yao, Q.; Jiao, Q.; Liu, B.; Chen, H. Polyepoxysuccinic Acid with Hyper-Branched Structure as an Environmentally Friendly Scale Inhibitor and Its Scale Inhibition Mechanism. *J. Saudi Chem. Soc.* **2019**, *23*, 61–74.
- (30) Liu, D.; Dong, W.; Li, F.; Hui, F.; Lédion, J. Comparative Performance of Polyepoxysuccinic Acid and Polyaspartic Acid on Scaling Inhibition by Static and Rapid Controlled Precipitation Methods. *Desalination* **2012**, *304*, 1–10.
- (31) He, C.; Tian, Z.; Zhang, B.; Lin, Y.; Chen, X.; Wang, M.; Li, F. Inhibition Effect of Environment-Friendly Inhibitors on the

- Corrosion of Carbon Steel in Recirculating Cooling Water. *Ind. Eng. Chem. Res.* **2015**, *54*, 1971–1981.
- (32) Zhang, B.; He, C.; Wang, C.; Sun, P.; Li, F.; Lin, Y. Synergistic Corrosion Inhibition of Environment-Friendly Inhibitors on the Corrosion of Carbon Steel in Soft Water. *Corros. Sci.* **2015**, *94*, 6–20.
- (33) Chen, Y.; Zhou, Y.; Yao, Q.; Nan, Q.; Zhang, M.; Sun, W. Inhibition, Dispersion and Corrosion Performance of a Novel Modified Polyepoxysuccinic Acid. *Desalin. Water Treat.* **2020**, *173*, 223–230.
- (34) Htet, T. T.; Zeng, D. Study on the Corrosion and Scale Inhibition Mechanism of the Thiourea-Modified Polyepoxysuccinic Acid (CNS-PESA). *J. Chem.* **2022**, *2022*, 1.
- (35) IRO Water. PESA Antiscalant Dispersant, PESA Polycarboxylic. <https://www.irowater.com/pesa-antiscalant-dispersant-pesa-polycarboxylic/> (accessed October 5, 2022).
- (36) Xiong, B.; Loss, R. D.; Shields, D.; Pawlik, T.; Hochreiter, R.; Zydney, A. L.; Kumar, M. Polyacrylamide Degradation and Its Implications in Environmental Systems. *npj Clean Water* **2018**, *1*, 2017.
- (37) Azzam, E. M. S.; El-Salam, H. M. A.; Mohamed, R. A.; Shaban, S. M.; Shokry, A. Control the Corrosion of Mild Steel Using Synthesized Polymers Based on Polyacrylamide. *Egypt. J. Pet.* **2018**, *27*, 897–910.
- (38) Chamovska, D.; Cvetkovska, M.; Grchev, T. Corrosion Inhibition of Iron in Hydrochloric Acid by Polyacrylamide. *J. Serbian Chem. Soc.* **2007**, *72*, 687–698.
- (39) Umoren, S. A.; Li, Y.; Wang, F. H. Influence of Iron Microstructure on the Performance of Polyacrylic Acid as Corrosion Inhibitor in Sulfuric Acid Solution. *Corros. Sci.* **2011**, *53*, 1778–1785.
- (40) Beniken, M.; Driouch, M.; Sfaira, M.; Hammouti, B.; Ebn Touhami, M.; Mohsin, M. A. Anticorrosion Activity of a Polyacrylamide with High Molecular Weight on C-Steel in Acidic Media: Part I. *J. Bio-Tribo-Corros.* **2018**, *4*, 1–14.
- (41) Wang, C.; Zou, C.; Cao, Y. Electrochemical and Isothermal Adsorption Studies on Corrosion Inhibition Performance of  $\beta$ -Cyclodextrin Grafted Polyacrylamide for X80 Steel in Oil and Gas Production. *J. Mol. Struct.* **2021**, *1228*, No. 129737.
- (42) Abd El-Lateef, H. M.; Gouda, M.; Shalabi, K.; Al-Omar, M. A.; Khalaf, M. M. Superhydrophobic Films-Based Nonanyl Carboxy Methylcellulose Grafted Polyacrylamide for AISI-Stainless Steel Corrosion Protection: Empirical Explorations and Computational Models. *J. Mol. Liq.* **2022**, *356*, No. 119063.
- (43) Biswas, A.; Mourya, P.; Mondal, D.; Pal, S.; Udayabhanu, G. Grafting Effect of Gum Acacia on Mild Steel Corrosion in Acidic Medium: Gravimetric and Electrochemical Study. *J. Mol. Liq.* **2018**, *251*, 470–479.
- (44) Ramesan, M. T.; Surya, K. Studies on Electrical, Thermal and Corrosion Behaviour of Cashew Tree Gum Grafted Poly-(Acrylamide). *Polym. Renewable Resour.* **2016**, *7*, 81–99.
- (45) Xiong, G.; Wu, Z.; Yi, J.; Fu, L.; Yang, Z.; Hsieh, C.; Yin, M.; Zeng, X.; Wu, C.; Lu, A.; Chen, X.; Hou, T.; Cao, D. ADMETlab 2.0: An Integrated Online Platform for Accurate and Comprehensive Predictions of ADMET Properties. *Nucleic Acids Res.* **2021**, *49*, W5–W14.
- (46) Dong, J.; Wang, N. N.; Yao, Z. J.; Zhang, L.; Cheng, Y.; Ouyang, D.; Lu, A. P.; Cao, D. S. ADMETlab: A Platform for Systematic ADMET Evaluation Based on a Comprehensively Collected ADMET Database. *Aust. J. Chem.* **2018**, *10*, 29.
- (47) Daina, A.; Michielin, O.; Zoete, V. SwissADME: A Free Web Tool to Evaluate Pharmacokinetics, Drug-Likeness and Medicinal Chemistry Friendliness of Small Molecules. *Sci. Rep.* **2017**, *7*, 42717.
- (48) SwissADME <http://swissadme.ch/index.php> (accessed May 1, 2021).
- (49) Delaney, J. S. ESOL: Estimating Aqueous Solubility Directly from Molecular Structure. *J. Chem. Inf. Comput. Sci.* **2004**, *44*, 1000–1005.
- (50) Hubin, A.; Terryn, H.; Mol, J. M. C.; Meeusen, M.; Visser, P.; Fern, L. The Use of Odd Random Phase Electrochemical Impedance Spectroscopy to Study Lithium-Based Corrosion Inhibition by Active Protective Coatings. *Electrochim. Acta* **2018**, *278*, 363–373.
- (51) Alamri, A. H.; Obot, I. B. Highly Efficient Corrosion Inhibitor for C1020 Carbon Steel during Acid Cleaning in Multistage Flash (MSF) Desalination Plant. *Desalination* **2019**, *470*, No. 114100.
- (52) Hasanin, M. S.; Al, S. A. Environmentally Benign Corrosion Inhibitors Based on Cellulose Niacin Nano-Composite for Corrosion of Copper in Sodium Chloride Solutions. *Int. J. Biol. Macromol.* **2020**, *161*, 345–354.
- (53) Abdel-Gaber, A. M.; Abd-El-Nabey, B. A.; Sidahmed, I. M.; El-Zayady, A. M.; Saadawy, M. Inhibitive Action of Some Plant Extracts on the Corrosion of Steel in Acidic Media. *Corros. Sci.* **2006**, *48*, 2765–2779.
- (54) Zarrouk, A.; Hammouti, B.; Lakhlifi, T.; Traisnel, M.; Vezin, H.; Bentiss, F. New 1 H-Pyrrole-2, 5-Dione Derivatives as Efficient Organic Inhibitors of Carbon Steel Corrosion in Hydrochloric Acid Medium: Electrochemical, XPS and DFT Studies. *Corros. Sci.* **2015**, *90*, 572–584.
- (55) Eduok, U.; Ohaeri, E.; Szpunar, J. Electrochemical and Surface Analyses of X70 Steel Corrosion in Simulated Acid Pickling Medium: Effect of Poly (N-Vinyl Imidazole ) Grafted Carboxymethyl Chitosan Additive. *Electrochim. Acta* **2018**, *278*, 302–312.
- (56) Pareek, S.; Jain, D.; Hussain, S.; Biswas, A.; Shrivastava, R.; Parida, S. K.; Kisan, H. K.; Lgaz, H.; Chung, I. M.; Behera, D. A New Insight into Corrosion Inhibition Mechanism of Copper in Aerated 3.5 Wt.% NaCl Solution by Eco-Friendly Imidazopyrimidine Dye: Experimental and Theoretical Approach. *Chem. Eng. J.* **2019**, *358*, 725–742.
- (57) Duvall, M.; Ayagou, D.; Tuyet, T.; Tran, M.; Tribollet, B.; Kittel, J.; Sutter, E.; Ferrando, N.; Mendibide, C.; Duret-thual, C. Electrochemical Impedance Spectroscopy of Iron Corrosion in H 2 S Solutions. *Electrochim. Acta* **2018**, *282*, 775–783.
- (58) Ech-Chihbi, E.; Nahle, A.; Salim, R.; Benhiba, F.; Moussaif, A.; El-hajjaji, F.; Ouddaa, H.; Guenboure, A.; Talebb, M.; Warad, I.; Zarrouk, A. Computational , MD Simulation, SEM / EDX and Experimental Studies for Understanding Adsorption of Benzimidazole Derivatives as Corrosion Inhibitors in 1 . 0 M HCl Solution. *J. Alloys Compd.* **2020**, *844*, No. 155842.
- (59) Parveen, M.; Mobin, M.; Zehra, S.; Aslam, R. L-Proline Mixed with Sodium Benzoate as Sustainable Inhibitor for Mild Steel Corrosion in 1M HCl : An Experimental and Theoretical Approach. *Sci. Rep.* **2018**, *8*, 7489.
- (60) Amin, M. A.; Khaled, K. F.; Fadl-allah, S. A. Testing Validity of the Tafel Extrapolation Method for Monitoring Corrosion of Cold Rolled Steel in HCl Solutions – Experimental and Theoretical Studies. *Corros. Sci.* **2010**, *52*, 140–151.
- (61) Morad, M. S. Inhibition of Iron Corrosion in Acid Solutions by Cefatrexyl: Behaviour near and at the Corrosion Potential. *Corros. Sci.* **2008**, *50*, 436–448.
- (62) Fischer, D. A.; Vargas, I. T.; Pizarro, G. E.; Armijo, F.; Walczak, M. The Effect of Scan Rate on the Precision of Determining Corrosion Current by Tafel Extrapolation: A Numerical Study on the Example of Pure Cu in Chloride Containing Medium. *Electrochim. Acta* **2019**, *313*, 457–467.
- (63) Obot, I. B.; Obi-egbedi, N. O. Fluconazole as an Inhibitor for Aluminium Corrosion in 0.1 M HCl. *Corros. Sci.* **2008**, *330*, 207–212.
- (64) Bashir, S.; Thakur, A.; Lgaz, H.; Chung, I.; Kumar, A. Corrosion Inhibition Efficiency of Bronopol on Aluminium in 0.5 M HCl Solution: Insights from Experimental and Quantum Chemical Studies. *Surf. Interfaces* **2020**, *20*, No. 100542.
- (65) Radwan, A. B.; Sliem, M. H.; Okonkwo, P. C.; Shibl, M. F.; Abdullah, A. M. Corrosion Inhibition of API X120 Steel in a Highly Aggressive Medium Using Stearamidopropyl Dimethylamine. *J. Mol. Liq.* **2017**, *236*, 220–231.
- (66) Farhadian, A.; Rahimi, A.; Safaei, N.; Shaabani, A.; Abdouss, M.; Alavi, A. A Theoretical and Experimental Study of Castor Oil-Based Inhibitor for Corrosion Inhibition of Mild Steel in Acidic Medium at Elevated Temperatures. *Corros. Sci.* **2020**, *175*, No. 108871.

(67) Chebabe, D.; About, S.; Damej, M.; Oubair, A.; Lakbaibi, Z.; Dermaj, A.; Benassaoui, H.; Doubi, M.; Hajjaji, N. Electrochemical and Theoretical Study of Corrosion Inhibition on Carbon Steel in 1M HCl Medium by 1,10-Bis(4-Amino-3-Methyl-1,2,4-Triazole-5-Thioyl)Decane. *J. Fail. Anal. Prev.* **2020**, *20*, 1673–1683.

(68) Lekka, M.; Andreatta, F.; Milošev, I.; Fedrizzi, L.; Rodi, P. The Synergistic Effect of Cerium Acetate and Sodium Sulphate on Corrosion Inhibition of AA2024-T3 at Various Temperatures. *Electrochim. Acta* **2021**, *370*, No. 137664.

(69) Abd-elaal, A. A.; Elbasiony, N. M.; Shaban, S. M.; Zaki, E. G. Studying the Corrosion Inhibition of Some Prepared Nonionic Surfactants Based on 3-(4-Hydroxyphenyl) Propanoic Acid and Estimating the Influence of Silver Nanoparticles on the Surface Parameters. *J. Mol. Liq.* **2018**, *249*, 304–317.

(70) Al-sodani, K. A. A.; Al-amoudi, O. S. B.; Maslehuddin, M.; Shameem, M. Efficiency of Corrosion Inhibitors in Mitigating Corrosion of Steel under Elevated Temperature and Chloride Concentration. *Constr. Build. Mater.* **2018**, *163*, 97–112.

(71) Singh, A. K.; Quraishi, M. A. Effect of Cefazolin on the Corrosion of Mild Steel in HCl Solution. *Corros. Sci.* **2010**, *52*, 152–160.

(72) Ben Aoun, S. On the Corrosion Inhibition of Carbon Steel in 1 M HCl with a Pyridinium-Ionic Liquid: Chemical, Thermodynamic, Kinetic and Electrochemical Studies. *RSC Adv.* **2017**, *7*, 36688–36696.

(73) Laamari, M. R.; Benzakour, J.; Berrekhis, F.; Derja, A.; Villemin, D. Adsorption and Corrosion Inhibition of Carbon Steel in Hydrochloric Acid Medium by Hexamethylenediamine Tetra-(Methylene Phosphonic Acid). *Arab. J. Chem.* **2016**, *9*, S245–S251.

(74) Wysocka, J.; Cieslik, M.; Krakowiak, S.; Ryl, J. Carboxylic Acids as Efficient Corrosion Inhibitors of Aluminium Alloys in Alkaline Media. *Electrochim. Acta* **2018**, *289*, 175–192.

(75) Goyal, M.; Vashist, H.; Kumar, S.; Bahadur, I.; Benhiba, F.; Zarrouk, A. Acid Corrosion Inhibition of Ferrous and Non-Ferrous Metal by Nature Friendly Ethoxycarbonylmethyltriphenylphosphonium Bromide (ECMTPB): Experimental and MD Simulation Evaluation. *J. Mol. Liq.* **2020**, *315*, No. 113705.

## Recommended by ACS

### Synergetic Effect of $\alpha$ -ZrP Nanosheets and Nitrogen-Based Flame Retardants on Thermoplastic Polyurethane

Sensen Han, Sherif Araby, *et al.*

MARCH 21, 2023  
ACS APPLIED MATERIALS & INTERFACES

READ 

### Design of Thermoplastic Polyurethanes with Conferred Antibacterial, Mechanical, and Cytotoxic Properties for Catheter Application

Rana Al Nakib, Franck Meyer, *et al.*

NOVEMBER 11, 2022  
ACS APPLIED BIO MATERIALS

READ 

### Synthesis of a Multielement Flame Retardant and Its Application in Epoxy Resin

Chao Wan, Huiru Ma, *et al.*

FEBRUARY 22, 2023  
ACS APPLIED POLYMER MATERIALS

READ 

### Fabrication of Hierarchical Patterned Surfaces Using a Functionalized CeO<sub>2</sub>-EPDM Composite for Crevice Corrosion Prevention on High-Voltage Insulators

Simpy Sanyal, Junsin Yi, *et al.*

NOVEMBER 04, 2022  
ACS OMEGA

READ 

Get More Suggestions >